

A microfluidic concentration gradient generator for simultaneous delivery of two reagents on a millimeter-sized sample

Milad Rismanian^a, Mohammad Said Saidi^{a*}, Navid Kashaninejad^b

^a Department of Mechanical Engineering, Sharif University of Technology, 11155-9567 Tehran, Iran

^b Queensland Micro- and Nanotechnology Centre, Griffith University, Nathan Campus, 170 Kessels Road, Brisbane, QLD 4111, Australia

* Corresponding author: mssaidi@sharif.edu, Tel.: +98 (21) 66165558

Abstract

Microfluidic concentration gradient generators (μ CGGs) are indispensable parts of many emerging lab-on-a-chip platforms for biological studies and drug delivery applications. Most of the μ CGGs reported in the literature can only generate the desired concentration gradients in a micron-sized sample (e.g., cells). As such, there is an unmet need to design a μ CGG that can generate continuous concentration gradients of multi reagents (e.g., drugs) in a millimeter-sized sample (e.g., tissue). Herein, we report the proof-of-concept of this class of μ CGG by combining a modified tree-like CGG with a micromixer. By conducting both experimental investigation and numerical analysis, we show that the proposed device can generate a continuous concentration gradient of two reagents and deliver all the possible combinations of their concentrations to a millimeter-sized sample. The proposed device can be used in a broad range of applications, especially ex-vivo drug chemosensitivity testing in personalized medicine.

Keywords: Micromixer, Concentration gradient generator, Microfluidics, Sensitivity analysis

Article Highlights

- Development of a new type of microfluidic concentration gradient generators (μ CGG)
- Millimeter-sized sample/Multi-reagents/ Continuous CGG
- The proposed μ CGG is highly suitable for drug delivery at a tissue level


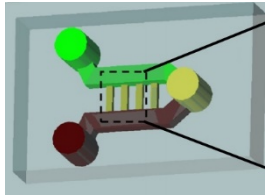
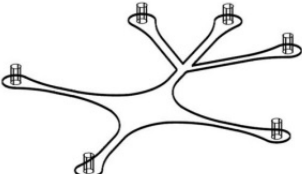
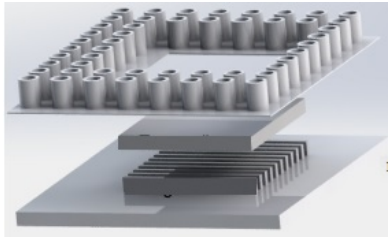
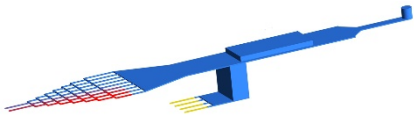
1. Introduction

Precise generating and controlling of concentration gradients of mass species are of paramount importance in various fields, including mechanical engineering [1,2], biology [3,4], pharmacology [5,6], chemical engineering [7,8], and toxicology [9]. Compared to conventional macroscale systems, microfluidic concentration gradient generators (μ CGGs) offers significant advantages and improvements [10,11]. For instance, μ CGGs can be integrated with various *in vitro* platforms to evaluate the effect of diverse phenomena, such as concentrations of different drugs, various chemical species on the cellular behaviour, and molecular concentrations on the porous media. [12-15]. For example, biomedical researchers expose their samples, e.g., cells, spheroids or tissues, to various drug doses using microfluidic platforms for drug delivery and discovery applications [16-18]. In addition, the chemical researchers use μ CGGs in mediums whose size can range from several microns to several millimeters to examine the diffusion phenomenon in porous membranes [19]. Furthermore, the vast majority of μ CGGs are designed to evaluate the effect of drugs in biological applications [20-22].

In general, almost all the μ CGGs that have been used in the literature can be categorized into four classes by considering the size of the sample, the number of chemical reagents, and continuous/discrete mode of the generated concentrations (Table 1).

These four classes of μ CGGs include: (1) Micron-sized sample/Mono-reagent/Discrete concentration gradient (CG); (2) Micron-sized sample/Mono-reagent/Continuous CG; (3) Micron-sized sample/Multi-reagents/Continuous CG; (4) Millimeter-sized sample/Mono-reagent/Discrete CG.

Table 1. General classes of the established μ CGGs reported in the literature compared to the μ CGG proposed in this study

	Size of sample		Number of reagents		CG class		Relevant research and its application
	Micrometer	Millimeter	1	>1	Discrete	Continuous	
1	•		•		•		 Biomedical research [23]
2	•		•			•	 Cell migration [24]
3	•			•		•	 Drug screening [25]
4		•	•		•		 Drug screening [26]
5		•		•		•	 Ex-vivo drug testing Current work

The main goal of the first class of μ CGG (micron-sized sample discrete devices) is to examine the effect of a single chemical reagent on a micron-sized sample. For instance, in biological applications, micron-sized samples (i.e., multicellular aggregates) are exposed to gradient

comprised of a limited number of diluted concentrations of a single specific drug, and the effects of the drug on the sample are studied [27]. This class of μ CGG has several limitations. First, it is not possible to test the effect of the drug on several millimeter-sized samples. Second, a simultaneous examination of the effect of two different reagents (e.g., two different drugs) is not feasible. Third, the system cannot generate a continuous chemical gradient. Since it is not possible to evaluate the effect of the predetermined chemical concentration using this class of μ CGG, the interpolation technique must be used to examine the effect of other desired concentrations.

The second class of μ CGG is designed to eliminate the third limitation of the first class. In this class, the chemical gradient of a single reagent can be generated in several micron areas in a continuous manner. So, all of the possible values of the chemical gradient can be generated, and their corresponding effects on the sample are observable [28,29,24].

The third class of microfluidic systems is designed to generate a continuous CG of multi-chemical reagents on a micrometre-sized sample [30-34,25]. Since this class of μ CGG generates a continuous concentration of the chemical species, the researchers can observe all of the desired chemical gradients. However, this class of μ CGG cannot generate the continuous range of the chemical gradients in a sample whose size is on the order of several millimeters. As such, this class of μ CGG is not suitable to evaluate most biological tissues (as a sample whose size is on the order of several millimeters) for *ex vivo* applications.

To address the limitation mentioned above, the fourth class of μ CGGs has been developed to deliver the concentration of chemicals to millimeter-sized samples. For example, Chang *et al.* designed a μ CGG to study the chemosensitivity of a drug (with different doses) on mouse brain slices, whose sizes were several millimeters [26]. Nevertheless, this class of μ CGG still entails the other limitations of other μ CGGs, i.e., these systems neither can simultaneously generate

concentration gradients of multi-chemical reagents nor can generate continuous chemical gradients.

Therefore, there is an unmet need to develop a new class of μ CGG that can rapidly generate continuous concentrations of more than one reagent on a millimeter-sized sample. To rapidly generate the desired concentration gradients on a relatively large area of the sample, the dimensionless Péclet (Pe) number (which is defined as $Pe=UL/D$, where U [m/s], L [m], and D [m²/s] are velocity, length and diffusion coefficient, respectively [35]), of the system should be carefully considered.

By considering the relative importance of Pe , all the four classes of μ CGGs can be further divided into two groups of diffusion ($Pe \ll 1$) and convection ($Pe \gg 1$) based μ CGGs. The relaxation times of diffusion-based and convection-based μ CGGs are defined as L^2/D and L/U , respectively. In the diffusion-based μ CGGs, a membrane is usually employed to connect the source of chemical reagents with the area where the desired gradients need to be generated [36]. Since the Pe is small in the diffusion-based μ CGGs, researchers use this system to generate concentration gradient in a large scale area. Nevertheless, these systems have a long relaxation time; thus, they are not appropriate for applications where rapid response is desirable. On the other hand, the convection-based μ CGGs are suitable to rapidly generate concentration gradient in a small area due to their short relaxation time and large Pe .

Herein, we present the design and fabrication of the fifth class of the μ CGGs, *viz.*, Millimeter-sized sample /Multi-reagents/ Continuous CG. To this aim, the μ CGG is developed based on mixed diffusion-convection-based approach ($Pe \approx 1$), in which, the mass transport is based on diffusion or convection in different parts of the system. This class of μ CGG can take advantage of both diffusion-based and convection-based μ CGGs to generate a synergistic effect and eliminate the individual limitations of each μ CGG. Compared to previous classes of μ CGGs developed in the literature, our proposed μ CGG can: (1) deliver two reagents simultaneously;

(2) generate a continuous concentration gradient of the two input reagents; and (3) deliver the reagents in an on-board sample whose size can be as large as several millimeters.

The μ CGG is evaluated both numerically and experimentally. The results show that a linear concentration gradient of first and second reagents can be generated in the sample along its width and length, respectively. In addition, the concentration gradient of the two reagents is equal to zero in the sample thickness. This behavior of device enables the researcher to benefit from the repeatability of the results in the sample thickness. The sensitivity results show that the correlation between the designed and working parameters is less than 0.3, leading to the repeatability of the presented data for other applications.

2. Materials and Methods

2.1. Device Operation

Fig. 1 schematically illustrates the principles of the operation of the proposed μ CGG to continuously generate the gradients of two reagents in several millimeter-sized samples. The sample width, length and thickness are defined along x, y and z direction shown in **Fig. 1**, respectively. The sample experiences all the possible combination of two reagents concentrations using this device. As shown in **Fig. 1**, the linear concentration gradient of the first reagent is prepared by a tree-like concentration gradient generator (CGG). We optimized the design of the tree-like CGG using the recently developed method by our group and was explained thoroughly in our previous publication [37]. In this method, a non-dimensional parameter is defined as the ratio of the minimum length required for the desired mixing to the product of the channel width and Peclet number which is constant for all micromixers in a CGG with the similar microchannel structure. So, knowing the value of this parameter (0.17 for serpentine microchannels), the minimum required length of all other micromixers in the CGG could be designed quickly and precisely.

This device is comprised of entirely modular and separate pieces which connected to each other. Two fluids, the first reagent and deionized water or buffer, enter into the tree-like CGG component, which is an entirely-independent microfluidic element used to generate a dilution gradient of the first reagents. The CGG component outputs nine discrete fluid outputs which are routed to the main microfluidics (MM) component using nine independent polytetrafluoroethylene (PTFE) tubes. The second reagent directly enters into four lower microchannel inputs of the MM. Second reagent entering from the lower microchannel acts as a mass source and generates a linear concentration gradient along the sample length (the y-direction).

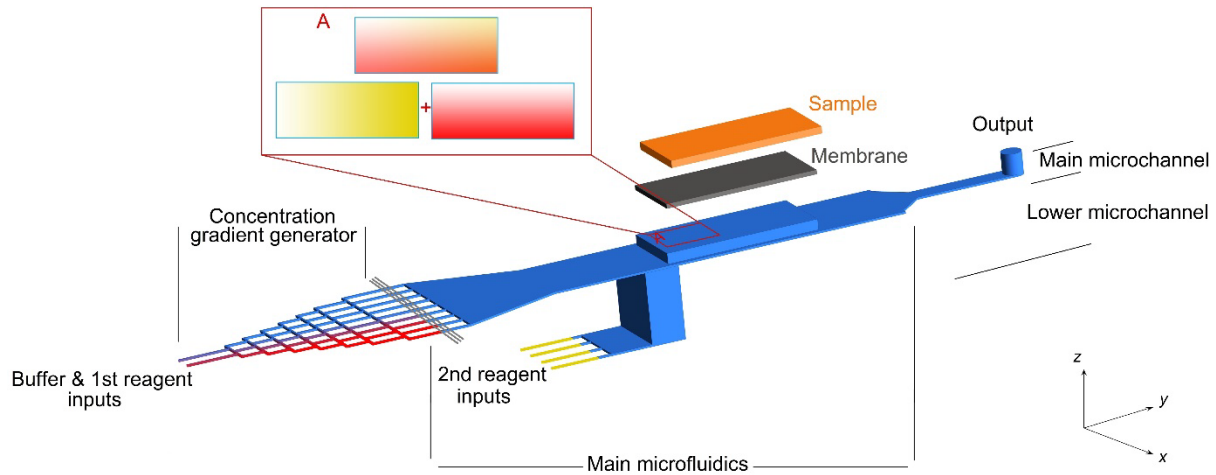


Fig.1. Schematic of the designed microfluidic device: The first reagent and buffer enter from upper entrance microchannel and the second reagent enter from lower entrance microchannel. These reagents are mixed in the main microchannel (MM) and then exit from the output. The sample is placed on the open-surface part of MM. Linear concentration distribution of the first reagent is generated using a tree-like CGG located between MM and syringe pump. As shown in surface A, two reagents concentrations combined on the sample to generate a linear concentration gradient of the first reagent along the sample width (the x-direction), and a linear concentration gradient of the second reagent along the sample length (the y-direction).

The proposed μ CGG combines two linear concentration gradients: (1) a linear concentration gradient of the first reagent along the sample width (the x-direction) generated by the tree-like CGG, and (2) a linear concentration gradient of the second reagent along the sample length (the y-direction) due to molecular diffusion of the second reagent contained in the lower microchannel input into the upper microchannel fluid sample. As such, all the possible

combinations of the two reagents can be tested on the sample using the proposed μ CGG . We also can replace the second reagent by water (or buffer in biological application) if it is desirable to evaluate the effects of concentration of one reagent on the sample.

2.2. Fabrication and Experimental Setup

The schematics of the experimental setup is shown in **Fig. 2**. The μ CGG consists of two microfluidic parts. The first part is the optimized tree-like CGG that was fabricated using standard soft lithography technique. The master mold of CGG was fabricated by Micromachining of polymethylmethacrylate (PMMA) which has an accuracy of 1 μ m. Then, polydimethylsiloxane-PDMS (Sigma-Aldrich, USA) was casted on the PMMA master mold to fabricate the CGG. Finally, The PDMS mold was placed in an oven at 90 C for 90 min and bonded to a standard microscope slide (Merck, Germany) via oxygen plasma treatment. The first microfluidic part is shown in Fig. 2 as CGG.

The second part of the μ CGG is a 5-layer PMMA microfluidic device fabricated using a 30W commercial CO₂ Epilog laser cutter. This fabricated part is shown in Fig. 2 as “main microfluidics”. In order to transfer drawings to the laser cutter, the CorelDraw software was used. The PMMA sheets were purchased from Cut Plastic Sheeting, UK. Absolute ethanol (Sigma-Aldrich, USA) was used as a solvent to bond the different PMMA layers together proposed by previous researchers [38]. The two microfluidic parts were separately fabricated so that the required modifications or replacements of each module could be performed separately.

A syringe pump was used to inject the fluids into the device with a certain velocity. Deionized water was injected with a flow rate of 4.5 μ l/min from one of the inlets of the tree-like CGG. At the same time, a dilute solution of Rhodamine B (Sigma-Aldrich, USA) with a concentration of 10^{-6} gr/gr-water and a flow rate of 4.5 μ l/min from the other inlet of the tree-

like CGG was infused. Concurrently, from each inlet of the second microfluidic device, we introduced four diluted solutions of fluorescein (Sigma-Aldrich, USA) with a concentration of 10^{-6} gr/gr-water and a flow rate of 2.0 $\mu\text{l}/\text{min}$. It should be noted that the syringe pumps, tree-like CGG, and second microfluidic device were connected by PTFE tubes with inner and outer diameters of 3.0 and 4.1 mm, respectively.

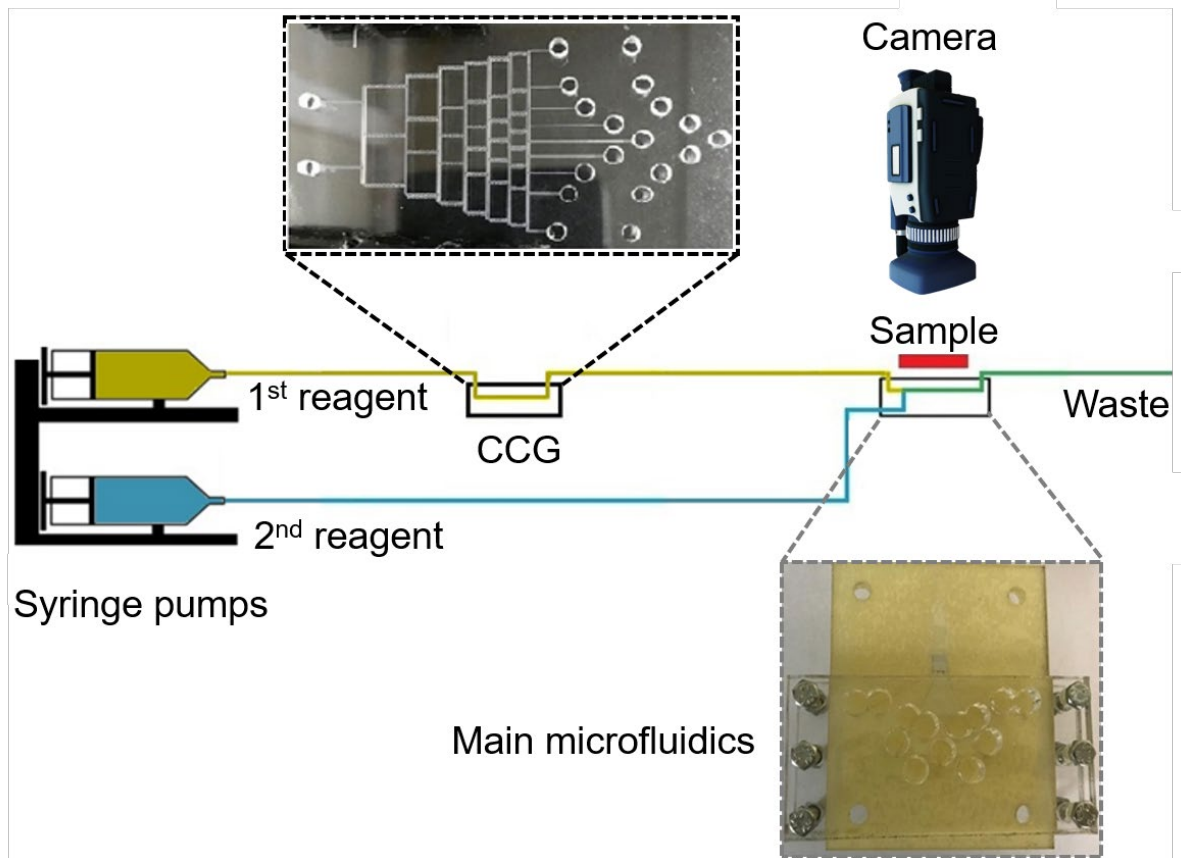


Fig. 2. The experimental setup for simultaneous generating of a continuous concentration gradient of two reagents on the millimeter-sized sample. The device consists of two parts. The first part is a tree-like CGG to generate a linear concentration distribution of the first reagent and the other one, called main microfluidics (MM), is a micromixer to mix the two reagents and deliver them to the sample. The fluids are injected into the device using two syringe pumps. The syringe pump, tree-like CGG, and MM are connected using PTFE tubes.

Since the main application of our microfluidic device is drug testing on human body, we used a coronal mouse brain slice of 300 μm in thickness as our porous sample. The purpose of selecting the mouse brain was only to expose a biological tissue as a porous medium. It should be noted that no drug or other biological test have been performed on the tissue. The sample was prepared from P9 neonatal mouse brain obtained from Cell-Electrophysiology Laboratory

of Tarbiat-Modares University, which is biologically very similar to the human brain [39]. The mouse brain slice (5 mm×5 mm×300 µm) was obtained with a Leica vibratome VT1000s (Leica Instruments, Germany). Then, the prepared sample was placed on a woven stainless steel membrane 316L with a mesh size of 30×30 (wires/inch), which was fixed at the above of MM. This grade of the stainless steel membrane is selected because of its biocompatibility and can be used in biological applications [40].

Finally, the concentrations of the two fluorescent fluids were analyzed by fluorescent images using an inverted microscope (Labomed TCM400, USA) and its fluorescent module (Labomed.Inc, USA), 4X and 10X objectives, a CCD camera (MD-30, Mshot co., China) and a x-y stage. The concentration distributions of the fluids were measured using the standard image processing technique with Matlab software.

2.3. Numerical Simulation

2.3.1. Mathematical Modelling

Numerical simulations based on the finite volume method were used to determine the fluid pattern and performance of the device. The governing equations are continuity, convection, and species diffusion equations, Eqs. (1-3), respectively. Assumptions are 3D flow, incompressible, Newtonian fluid and laminar flow. According to hydraulic diameters of tree-like CGG and the main microfluidic channels (0.3 and 3.1 mm, respectively) and the values of flow rates, the flow is in the laminar regime for both parts.

$$\frac{\partial u_i}{\partial x_i} = 0 \quad (1)$$

$$\rho \left[\frac{\partial u_i}{\partial t} + u_j \frac{\partial u_i}{\partial x_j} \right] = -\frac{\partial p}{\partial x_i} + \mu \frac{\partial^2 u_i}{\partial x_j \partial x_j} \quad (2)$$

$$\frac{\partial C_m}{\partial t} + u_i \frac{\partial C_m}{\partial x_i} = D_m \frac{\partial^2 C_m}{\partial x_i \partial x_i} \quad (3)$$

where, t [s], u [m/s], ρ [kg/m³], μ [kg/m.s], C_i [-] and D_i [m²/s] are time, velocity, density, pressure, viscosity and dimensionless concentration and diffusion coefficient of m^{th} species, respectively. To predict the mass transfer in the sample and woven stainless steel membrane, Eq. (4) as convection equation in porous media is replaced with Eq. 2 [41,42].

$$\frac{\rho}{\varepsilon} \left[\frac{\partial u_i}{\partial t} + u_j \frac{\partial u_i}{\partial x_j} \right] = - \frac{\partial p}{\partial x_i} + \frac{\mu}{\varepsilon} \frac{\partial^2 u_i}{\partial x_j \partial x_j} - \left[\frac{\mu}{K} u_i + \frac{1}{2} B \sqrt{u_i^2} \rho u_i \right] \quad (4)$$

where, ε [-], K [m²] and B [m⁻¹] are porosity, permeability, and inertial pressure loss coefficient of porous media, respectively. The simulation is performed with Ansys-Fluent 16.2 software.

2.3.2 Boundary Conditions

The boundary conditions (BCs) for solving the governing equations are listed in Table 2.

Table 2. Applied BCs for the numerical simulation of the μ CGG

Input/output	Boundary conditions
Outlets	Pressure outlet
The MM upper input microchannel	$C_1=(0-1)$ linearly
	$C_2=0$
	$\dot{m}_1 = 1.67 \times 10^{-8} \text{ kg / s}$
The MM lower input microchannel	$C_1=0$
	$C_2=1$
	$\dot{m}_2 = 3.20 \times 10^{-8} \text{ kg / s}$
Walls	$u=0$ (no-slip BC)

The diffusion coefficient of two species, Rhodamine B and Fluorescein in the water at 25°C are $4.27 \times 10^{-10} \text{ m}^2/\text{s}$ and $4.25 \times 10^{-10} \text{ m}^2/\text{s}$, respectively [43]. Density and viscosity of water at 25°C are $1 \times 10^3 \text{ kg/m}^3$ and $1 \times 10^{-3} \text{ kg/m.s}$, respectively. The porous media coefficients of the sample and woven stainless steel are listed in Table 3.

Table 3. Porosity, permeability and inertial pressure loss coefficient in the sample and woven stainless steel membrane

	Value		Reference
Membrane 30×30	ε	0.76	[44]
	K [m ²]	1.69×10^{-10}	
Sample	ε	0.4	[26,45]
	K [m ²]	10^{-11}	

2.4 Sensitivity Analysis

We use sensitivity analysis to estimate how small changes of the input variables can affect the performance of the proposed μ C GG. Some small variations in the performance of syringe pump, the sample specification and diffusion coefficient of the reagents are possible due to reusing the device for a new test. So, we listed the input/output parameters in Table 4.

Table 4. Input/output parameters in sensitivity analyzing of the proposed μ C GG

Input parameters	Output parameter
\dot{m}_1	
\dot{m}_2	
$(I/K)_{\text{sample}}$	A
$(\varepsilon)_{\text{sample}}$	
D_1	
D_2	

The output parameter, α , is defined as:

$$\alpha = \sqrt{\frac{\sum_{\text{surface}=1}^4 (\bar{c}_1 - \bar{c}_{1-dp})^2 + \sum_{\text{surface}=1}^4 (\bar{c}_2 - \bar{c}_{2-dp})^2}{8}} \quad (5)$$

where, \bar{c} is the average concentration of reagent on four peripheral surfaces of the sample. The subscriptions 1 , 2 and dp refer to the first reagent, second reagent, and design-point conditions, respectively. Each of the input parameters changed by no more than 10% of their initial values. Then, the output parameter is calculated to investigate the effect of the input parameters on the device performance.

3. Results and Discussion

3.1. Numerical Results

3.1.1 Velocity Profiles

To examine the velocity behaviour of the fluid inside the MM channel, the velocity contours obtained from numerical simulation are presented (**Fig. 3**). The cross-sectional view in Fig.3 shows the velocity distribution throughout the device. The presence of the woven stainless steel membrane (as a porous media) causes the fluids to flow in the direction of the sample thickness (the z-direction) through diffusion. Since mass diffusion is the primary mechanism for the reagent transport from the MM to the sample, the velocity in the membrane is much smaller than its value in the MM. The ratio of the calculated average velocity in the porous membrane to the MM is approximately 0.02. As explained in the introduction, employing both the tree-like CGG and the MM in the device has the advantage of producing a concentration gradient in several millimeter-sized samples. On top of that, it can rapidly generate the desired concentrations throughout the sample.

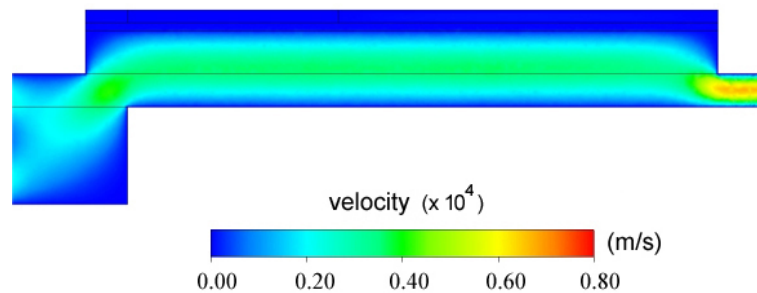


Fig. 3. Velocity contour in the middle cross-sectional plane of the MM obtained from the numerical simulation.

3.1.2. Concentration Distributions of the Reagents at the Middle Cross-Sectional Plane of the Main Microfluidics (MM)

The concentration distributions of the reagents in the MM are shown in **Fig. 4**, both quantitatively and qualitatively. **Fig. 4a-c** shows the contour of two reagents distribution in the cross-sectional plane of the MM obtained from the numerical simulation. The diffusion

coefficient of the first and second reagents are assumed to be $4.27 \times 10^{-10} \text{ m}^2/\text{s}$ and $4.25 \times 10^{-10} \text{ m}^2/\text{s}$, respectively. The input microchannel of the second reagent, MM, the output microchannel, the woven stainless steel membrane, and the sample are shown in this part of the figure from down to up, respectively. The important role of the main microfluidics is to mix the two reagents. The concentrations of first and second reagents are constant along the thickness of the sample (the z-direction) with a qualitative consideration of the figure. The zero concentration gradient of the reagents is an important advantage of the device, especially for biological applications.

The main advantage of our μCGG over previously proposed ones is its ability to generate continuous concentration variation of the two reagents on the sample. This advantage eliminates the spatial interpolation needed to estimate the sample behaviour against different concentrations of reagents. In our proposed μCGG , all possible concentrations of the reagents are directly observable on the sample.

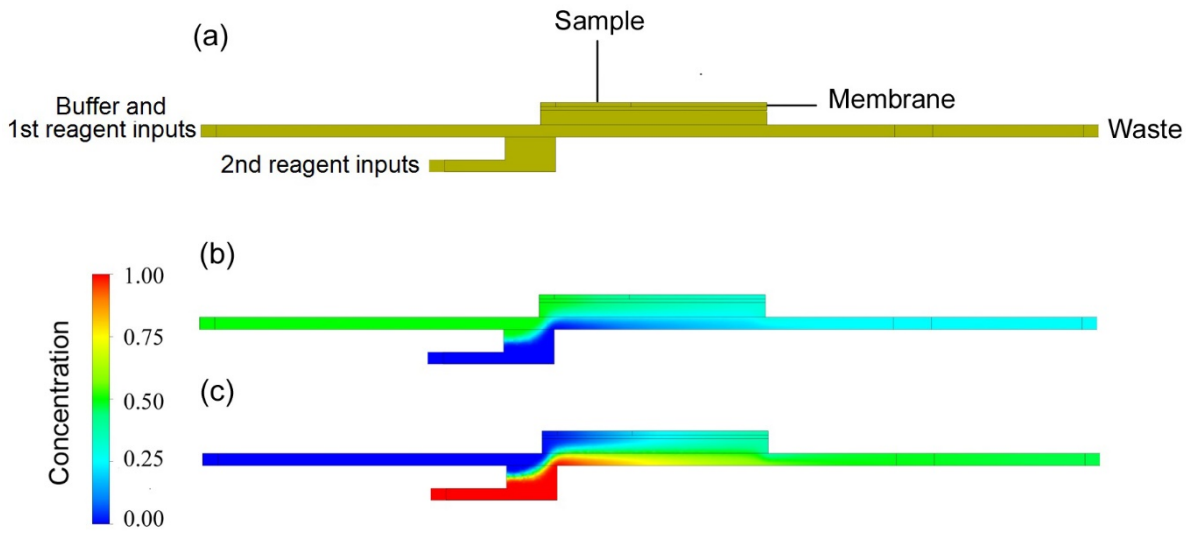


Fig. 4. Concentration distributions of both reagents obtained from numerical simulation, a: The cross-sectional plane of the MM at the middle plane of the microfluidic device, b: The concentration contours of the first reagent in the plane, c: The concentration contours of the second reagent in the plane; The diffusion coefficient of the first and second reagents are assumed to be $4.27 \times 10^{-10} \text{ m}^2/\text{s}$ and $4.25 \times 10^{-10} \text{ m}^2/\text{s}$, respectively.

3.2 Experimental Results

In **Fig. 5a-b** the concentrations of first and second reagents are plotted against the sample width from experimental results. The concentration variations with sample width is shown in three locations along the sample length; $y=0$ mm at the sample inlet, $y=2.5$ mm at the middle and $y=5$ mm at the sample outlet. As shown in this figure the sample experiences an approximately linear concentration gradient of first and second reagents in the directions of the sample width and length, respectively. The differences between the values of numerical simulations and experiments are also shown in **Fig. 5a-b** by error bars. The maximum relative errors are 5.9% and 9.1%, respectively. This figure shows that there is a good agreement between the numerical simulation and experimental data.

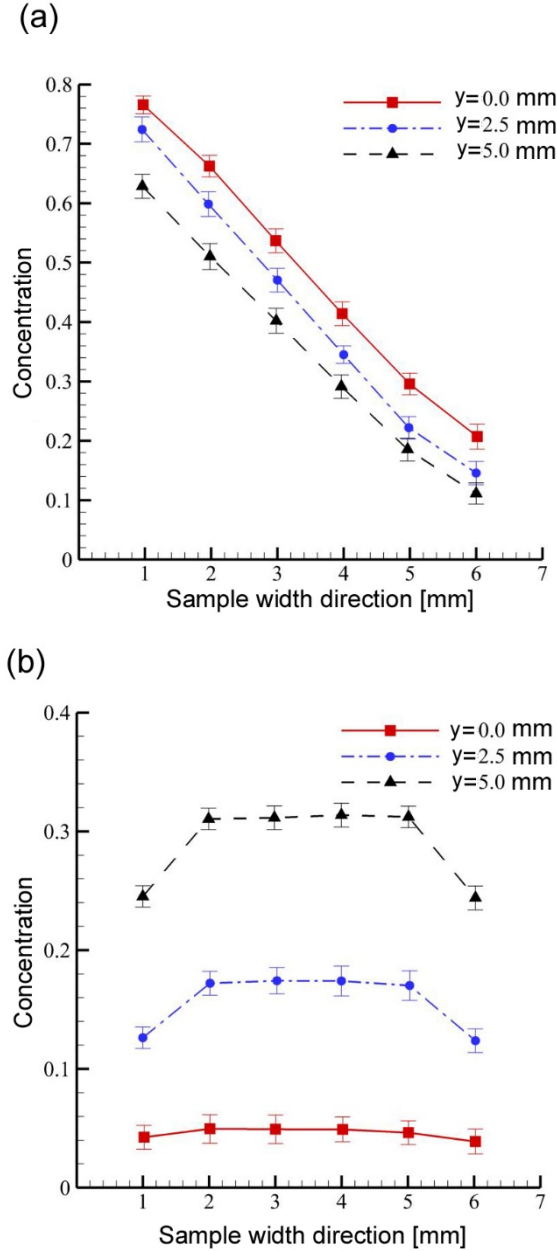


Fig. 5. The concentration distributions of both reagents along the sample width obtained from numerical simulation and experimental analysis, a: The concentration of the first reagent, b: The concentration of the second reagent. The error bars show the difference between the numerical simulation and experimental data.

The results show that the average concentration of the first reagent decreases along y-direction because of its dilution with the second reagent entering MM. The concentration of the second reagent is approximately constant in sample width direction except on its peripheral edges ($x=1$ mm and $x=6$ mm). These changes are because of the wall effect, which pushed the second

reagent to the center of MM ($x=3.5$ mm). The smaller sample could be placed on the center of MM width to achieve a constant concentration of the second reagent in the x-direction.

3.3 Relaxation Time

It is of great interest to change the applied reagent concentrations on the sample during the experiments. For example, in biological applications, it is desired to change the drug doses applied to the sample during the experiments. It is also important to obtain the average concentration of the drug in the sample to reach its steady condition in a reasonable time. So, it is an advantage for a microfluidic device to have this capability. To estimate the relaxation time of the proposed μ CGG, we used an unsteady numerical simulation of the microfluidics with a time scale equal to $0.1(L^2/D) \approx 20$ sec. The relaxation time is defined as the time that the system reaches 95 percent of its steady condition.

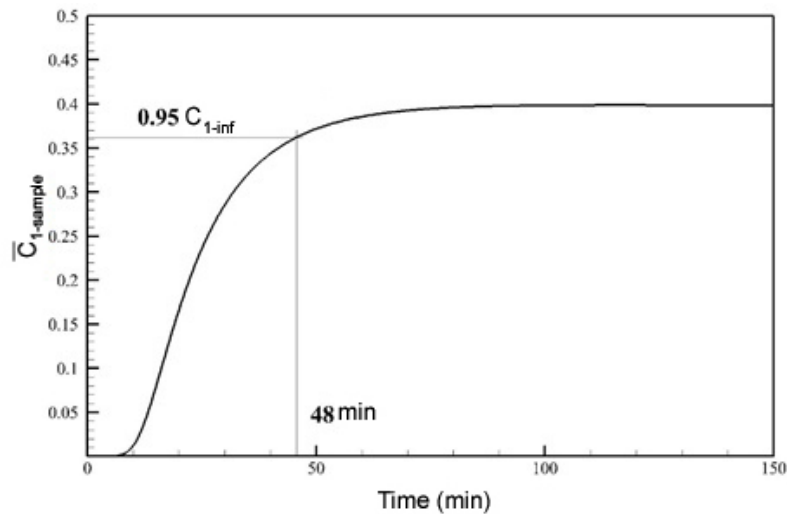


Fig. 6. The average concentration of the first reagent in the sample versus time (obtained from numerical simulations). The average concentration of the first reagent reaches 95% of steady-state conditions in 48 min.

In **Fig. 6**, the average concentration of the first reagent in the sample is plotted versus time from the numerical simulation. According to this figure, the relaxation time of the μ CGG is 48 minutes. Therefore, this is a limitation for using this μ CGG for applications in which experiment duration time is comparable to the relaxation time. On the other hand, for

applications in which the sample exposure time is approximately 1~2 days (such as drug discovery), the relaxation time of the proposed μ CGG is only 3% of the experimental duration. So, the proposed μ CGG responds fast to any concentration change in the experiments where the test duration time is much longer than the estimated relaxation time.

3.4. The Effects of Varying the Sample Thickness

The selection of large sample thickness is important for the researchers, especially for biologists, due to two reasons. Firstly, the behaviour of a single cell exposing to a specific concentration of a drug is different from that of a tissue due to extracellular interactions. So, they are interested in using tissue scale thickness rather than cell size, the point that is applicable in our proposed μ CGG, using animal tissue or even patient-derived xenografts in line with personalized medicine. Secondly, the experiment should be repeated in a fixed condition to obtain the average results because of inhomogeneous statistics. Because of zero concentration gradient of reagents in the sample thickness, multiple images can be captured at different thicknesses in a sample using confocal microscopy.

In order to prove that the concentration of the reagents is constant along the sample thickness, we compute the relative percentage error due to substitute the concentration on the upper surface of the sample instead of the mean concentration between the upper and lower surface of the sample using numerical simulation. In **Fig. 7a** and **Fig. 7b** contours of this relative percentage error for first and second reagents, respectively. The mean concentration of the reagent is defined as $C_{mean} = (C_{up} + C_{down}) / 2$ which C_{up} and C_{down} are the concentration of the reagent on the upper and lower surface of the sample, respectively. The relative percentage error is computed by $\left[(C_{up} - C_{middle}) / C_{middle} \right] \times 100\%$. The maximum relative percent error for the first middle and second reagents are 1.93% and 1.31%, respectively; therefore, the concentration gradient of both reagents along the sample thickness is sufficiently small, near

0%, such that researchers could benefit from this near-ideal gradient to take their required data by moving along sample thickness.

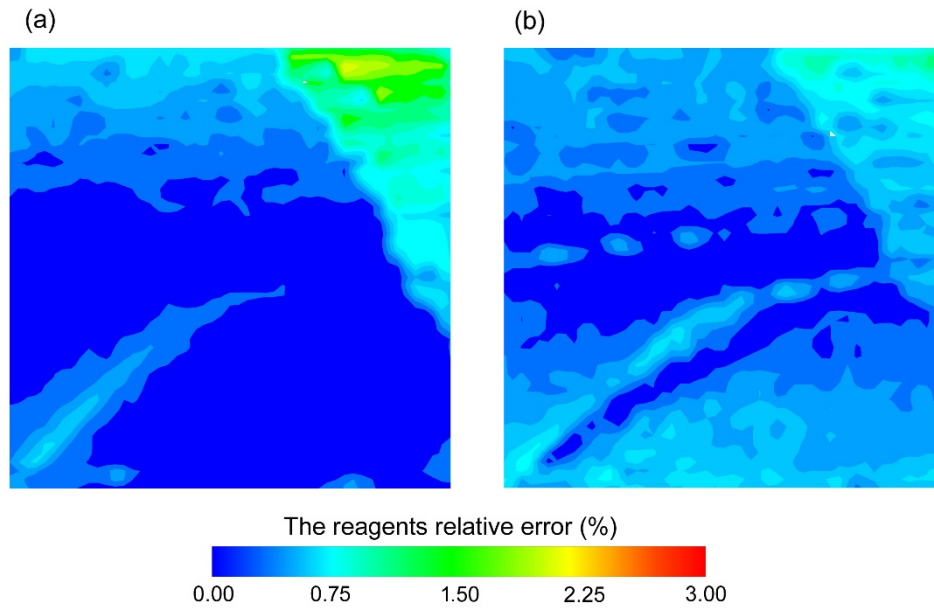


Fig. 7. The relative percentage error due to substituting the concentration on the sample upper surface instead of the middle surface, a: relative error for the first reagent, b: relative error for second reagent (obtained from numerical simulations)

3.5 Sensitivity Analysis

The sensitivity of the output parameter versus the input parameters, Table 4, was considered to in this section. In the process of using the μ CGG, the test conditions can be changed from an experiment to another. For example, porosity and permeability of the patient-derived tissue (as the sample) may significantly vary from one patient to another. Also, the diffusivity of the drugs (due to switching to other classes of drugs) and their flow rate will be substantially different. Therefore, it is necessary to examine the sensitivity of the performance of the proposed μ CGG as a function of the above parameters.

In this regard, a set of 60 simulations is performed, and the output parameter is calculated using **Eq. 5**. In **Fig. 8**, the sensitivity and correlation of the output parameter versus the input parameters are shown. Since the correlation of the output parameter to each input parameter is less than 0.3, changes of values of output parameters will not affect the performance of the

device. In other words, possible changes in test conditions such as variability of the sample's porosity and permeability, as well as diffusivity of different drugs, will not significantly affect the predicted concentration distribution of the reagents throughout the sample.

In addition, this figure indicates that the μ CGG has the most sensitivity relative to the mass flow of the first reagent. Thus, it is important to control the error of the syringe pump if the class of the sample (e.g., its porosity and permeability) and the chemical reagents are fixed.

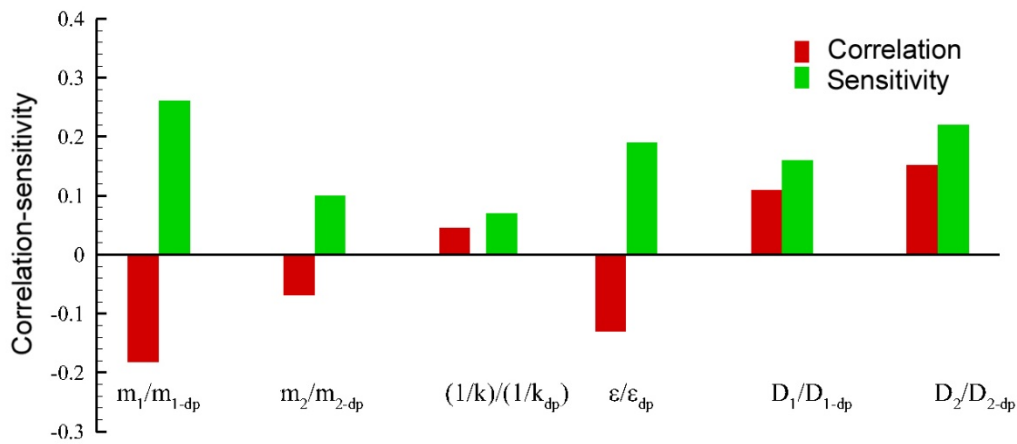


Fig. 8. The input and output parameters correlation, the sensitivity of the output parameter versus the input parameters

4 Conclusion

The main goal of this paper was to devise a microfluidic device for simultaneously generating the concentration gradients of two reagents in several millimeter-sized samples. To this aim, we employed both a modified tree-like CGG and a micromixer. Accordingly, we used numerical, experimental tests and sensitivity analysis to study the performance of the designed microfluidic device. According to results, the sample could be exposed to a linear concentration gradient of the chemical reagents along the width and length of the sample. The combination of two microfluidic parts, i.e., the CGG and micromixer, causes the designed device to generate a continuous concentration gradient. Also, since the concentration of the two reagents is constant along the sample's thickness, it is possible to obtain the desired data in the direction

of the thickness using a confocal microscopy technique (z-stacking) for statistical analysis. So, the proposed device allows the examination of the effect of a continuous range of variations of the concentrations of two reagents (e.g., drugs) and their combinations on samples (e.g., tissues). The proposed μ CGG can be of great interest in various fields of science, especially ex-vivo drug chemosensitivity testing in personalized medicine.

Acknowledgment

We would like to express our great appreciation to Dr. Javad Mirnajafizadeh, head of Cell-Electrophysiology Laboratory of Tarbiat-Modares University, for providing the neonatal mouse brain and the vibratome slicer.

Compliance with ethical standards

Conflict of interest

The authors declare no conflict of interest.

References

1. Bordbar A, Kheirandish S, Taassob A, Kamali R, Ebrahimi A (2020) High-viscosity liquid mixing in a slug-flow micromixer: a numerical study. *Journal of Flow Chemistry*:1-11. doi:[10.1007/s41981-020-00085-7](https://doi.org/10.1007/s41981-020-00085-7)
2. Qian J-y, Li X-j, Gao Z-x, Jin Z-j (2019) Mixing efficiency and pressure drop analysis of liquid-liquid two phases flow in serpentine microchannels. *Journal of Flow Chemistry* 9 (3):187-197. doi:[10.1007/s41981-019-00040-1](https://doi.org/10.1007/s41981-019-00040-1)
3. Žnidaršič-Plazl P (2017) Biotransformations in microflow systems: Bridging the gap between academia and industry. *Journal of Flow Chemistry* 7 (3-4):111-117. doi:[10.1556/1846.2017.00021](https://doi.org/10.1556/1846.2017.00021)
4. Sonnen KF, Merten CA (2019) Microfluidics as an emerging precision tool in developmental biology. *Developmental cell* 48 (3):293-311. doi:[10.1016/j.devcel.2019.01.015](https://doi.org/10.1016/j.devcel.2019.01.015)
5. Hajba L, Guttman A (2017) Continuous-flow-based microfluidic systems for therapeutic monoclonal antibody production and organ-on-a-chip drug testing. *Journal of Flow Chemistry* 7 (3-4):118-123. doi:[10.1556/1846.2017.00014](https://doi.org/10.1556/1846.2017.00014)
6. Menon NV, Lim SB, Lim CT (2019) Microfluidics for personalized drug screening of cancer. *J Current opinion in pharmacology* 48:155-161. doi:[10.1016/j.coph.2019.09.008](https://doi.org/10.1016/j.coph.2019.09.008)
7. López COC, Fejes Z, Viskolcz B (2019) Microreactor assisted method for studying isocyanate–alcohol reaction kinetics. *Journal of Flow Chemistry* 9 (3):199-204. doi:[10.1007/s41981-019-00041-0](https://doi.org/10.1007/s41981-019-00041-0)
8. Jankowski P, Kutaszewicz R, Ogończyk D, Garstecki P (2019) A microfluidic platform for screening and optimization of organic reactions in droplets. *Journal of Flow Chemistry*:1-12. doi:[10.1007/s41981-019-00055-8](https://doi.org/10.1007/s41981-019-00055-8)
9. Ng WL, Yeong WY (2019) The future of skin toxicology testing–3D bioprinting meets microfluidics. *J Int J Bioprinting* 5:237. doi:[10.18063/ijb.v5i2.1.237](https://doi.org/10.18063/ijb.v5i2.1.237)
10. Wang X, Liu Z, Pang Y (2017) Concentration gradient generation methods based on microfluidic systems. *RSC Advances* 7 (48):29966-29984. doi:[10.1039/C7RA04494A](https://doi.org/10.1039/C7RA04494A)
11. Ebadi M, Moshksayan K, Kashaninejad N, Saidi MS, Nguyen N-T (2020) A tool for designing tree-like concentration gradient generators for lab-on-a-chip applications. *Chemical Engineering Science* 212:115339. doi:[10.1016/j.ces.2019.115339](https://doi.org/10.1016/j.ces.2019.115339)
12. Du Y, Shim J, Vidula M, Hancock MJ, Lo E, Chung BG, Borenstein JT, Khabiry M, Cropek DM, Khademhosseini A (2009) Rapid generation of spatially and temporally controllable long-range concentration gradients in a microfluidic device. *Lab on a Chip* 9 (6):761-767. doi:[10.1039/B815990D](https://doi.org/10.1039/B815990D)
13. He YJ, Young DA, Mededovic M, Li K, Li C, Tichauer K, Venerus D, Papavasiliou G (2018) Protease-Sensitive Hydrogel Biomaterials with Tunable Modulus and Adhesion Ligand Gradients for 3D Vascular Sprouting. *Biomacromolecules* 19 (11):4168-4181. doi:[10.1021/acs.biomac.8b00519](https://doi.org/10.1021/acs.biomac.8b00519)
14. Perestrelo A, Águas A, Rainer A, Forte G (2015) Microfluidic organ/body-on-a-chip devices at the convergence of biology and microengineering. *Sensors* 15 (12):31142-31170. doi:[10.3390/s151229848](https://doi.org/10.3390/s151229848)
15. Ross A, Pompano R (2018) Diffusion of cytokines in live lymph node tissue using microfluidic integrated optical imaging. *Analytica chimica acta* 1000:205-213. doi:[10.1016/j.aca.2017.11.048](https://doi.org/10.1016/j.aca.2017.11.048)
16. Bower R, Green VL, Kuvshinova E, Kuvshinov D, Karsai L, Crank ST, Stafford ND, Greenman J (2017) Maintenance of head and neck tumor on-chip: gateway to personalized treatment? *Future science OA* 3 (2):FSO174. doi:[10.4155/fsoa-2016-0089](https://doi.org/10.4155/fsoa-2016-0089)
17. Masuda T, Song W, Nakanishi H, Lei W, Noor AM, Arai F (2017) Rare cell isolation and recovery on open-channel microfluidic chip. *PloS one* 12 (4):e0174937. doi:[10.1371/journal.pone.0174937](https://doi.org/10.1371/journal.pone.0174937)
18. Moghadas H, Saidi MS, Kashaninejad N, Nguyen N-T (2018) Challenge in particle delivery to cells in a microfluidic device. *Drug Delivery and Translational Research* 8 (3):830-842. doi:[10.1007/s13346-017-0467-3](https://doi.org/10.1007/s13346-017-0467-3)

19. Gerami A, Alzahid Y, Mostaghimi P, Kashaninejad N, Kazemifar F, Amirian T, Mosavat N, Ebrahimi Warkiani M, Armstrong RT (2019) Microfluidics for Porous Systems: Fabrication, Microscopy and Applications. *Transport in Porous Media* 130 (1):277-304. doi:[10.1007/s11242-018-1202-3](https://doi.org/10.1007/s11242-018-1202-3)
20. Meijer TG, Naipal KA, Jager A, van Gent DC (2017) Ex vivo tumor culture systems for functional drug testing and therapy response prediction. *Future science OA* 3 (2):FSO190. doi:[10.4155/fsoa-2017-0003](https://doi.org/10.4155/fsoa-2017-0003)
21. Sweet EC, Chen JC-L, Karakurt I, Long AT, Lin L 3D printed three-flow microfluidic concentration gradient generator for clinical E. coli-antibiotic drug screening. In: 2017 IEEE 30th International Conference on Micro Electro Mechanical Systems (MEMS), 2017. IEEE, pp 205-208
22. Astolfi M, Péant B, Lateef M, Rousset N, Kendall-Dupont J, Carmona E, Monet F, Saad F, Provencher D, Mes-Masson A-MJLoaC (2016) Micro-dissected tumor tissues on chip: an ex vivo method for drug testing and personalized therapy. *Lab on a Chip* 16 (2):312-325. doi:[10.1039/C5LC01108F](https://doi.org/10.1039/C5LC01108F)
23. Ye N, Qin J, Shi W, Liu X, Lin B (2007) Cell-based high content screening using an integrated microfluidic device. *Lab on a Chip* 7 (12):1696-1704. doi:[10.1039/B711513J](https://doi.org/10.1039/B711513J)
24. Saadi W, Rhee SW, Lin F, Vahidi B, Chung BG, Jeon NL (2007) Generation of stable concentration gradients in 2D and 3D environments using a microfluidic ladder chamber. *Biomedical microdevices* 9 (5):627-635. doi:[10.1007/s10544-007-9051-9](https://doi.org/10.1007/s10544-007-9051-9)
25. Mitxelena-Iribarren O, Zabalo J, Arana S, Mujika M (2019) Improved microfluidic platform for simultaneous multiple drug screening towards personalized treatment. *Biosensors and Bioelectronics* 123:237-243. doi:[10.1016/j.bios.2018.09.001](https://doi.org/10.1016/j.bios.2018.09.001)
26. Chang TC, Mikheev AM, Huynh W, Monnat RJ, Rostomily RC, Folch A (2014) Parallel microfluidic chemosensitivity testing on individual slice cultures. *Lab on a Chip* 14 (23):4540-4551. doi:[10.1039/C4LC00642A](https://doi.org/10.1039/C4LC00642A)
27. Hong B, Xue P, Wu Y, Bao J, Chuah YJ, Kang Y (2016) A concentration gradient generator on a paper-based microfluidic chip coupled with cell culture microarray for high-throughput drug screening. *Biomedical microdevices* 18 (1):21. doi:[10.1007/s10544-016-0054-2](https://doi.org/10.1007/s10544-016-0054-2)
28. Wang Y, Mukherjee T, Lin Q (2006) Systematic modeling of microfluidic concentration gradient generators. *Journal of Micromechanics and Microengineering* 16 (10):2128
29. Guermontprez C, Michelin S, Baroud CN (2015) Flow distribution in parallel microfluidic networks and its effect on concentration gradient. *Biomicrofluidics* 9 (5):054119. doi:[10.1063/1.4932305](https://doi.org/10.1063/1.4932305)
30. Saadi W, Wang S-J, Lin F, Jeon NL (2006) A parallel-gradient microfluidic chamber for quantitative analysis of breast cancer cell chemotaxis. *Biomedical microdevices* 8 (2):109-118. doi:[10.1007/s10544-006-7706-6](https://doi.org/10.1007/s10544-006-7706-6)
31. Lin F, Saadi W, Rhee SW, Wang S-J, Mittal S, Jeon NL (2004) Generation of dynamic temporal and spatial concentration gradients using microfluidic devices. *Lab on a Chip* 4 (3):164-167. doi:[10.1039/B313600K](https://doi.org/10.1039/B313600K)
32. Dertinger SK, Chiu DT, Jeon NL, Whitesides GM (2001) Generation of gradients having complex shapes using microfluidic networks. *Analytical Chemistry* 73 (6):1240-1246. doi:[10.1021/ac001132d](https://doi.org/10.1021/ac001132d)
33. Yang C-G, Wu Y-F, Xu Z-R, Wang J-H (2011) A radial microfluidic concentration gradient generator with high-density channels for cell apoptosis assay. *Lab on a Chip* 11 (19):3305-3312. doi:[10.1039/C1LC20123A](https://doi.org/10.1039/C1LC20123A)
34. Glawdel T, Elbukun C, Lee LE, Ren CL (2009) Microfluidic system with integrated electroosmotic pumps, concentration gradient generator and fish cell line (RTgill-W1)—towards water toxicity testing. *Lab on a Chip* 9 (22):3243-3250. doi:[10.1039/B911412M](https://doi.org/10.1039/B911412M)
35. Toh AG, Wang Z, Yang C, Nguyen N-T (2014) Engineering microfluidic concentration gradient generators for biological applications. *Microfluidics and nanofluidics* 16 (1-2):1-18. doi:[10.1007/s10404-013-1236-3](https://doi.org/10.1007/s10404-013-1236-3)

36. Atencia J, Morrow J, Locascio LE (2009) The microfluidic palette: a diffusive gradient generator with spatio-temporal control. *Lab on a Chip* 9 (18):2707-2714. doi:[10.1039/B902113B](https://doi.org/10.1039/B902113B)
37. Rismanian M, Saidi MS, Kashaninejad N (2019) A new non-dimensional parameter to obtain the minimum mixing length in tree-like concentration gradient generators. *Journal of Chemical Engineering Science* 195:120-126. doi:[10.1016/j.ces.2018.11.041](https://doi.org/10.1016/j.ces.2018.11.041)
38. Ongaroa AE, Howartha N, La Carrubac V, Kersaudy-Kerhoas M Rapid Prototyping for Micro-engineering and Microfluidic Applications: Recycled PMMA, a Sustainable Substrate Material. In: *Advances in Manufacturing Technology XXXII: Proceedings of the 16th International Conference on Manufacturing Research*, 2018. IOS Press, p 107
39. Sheldon RA, Windsor C, Ferriero DM (2018) Strain-Related Differences in Mouse Neonatal Hypoxia-Ischemia. *J Developmental neuroscience* 40 (5-6):490-496. doi:[10.1159/000495880](https://doi.org/10.1159/000495880)
40. Muley SV, Vidvans AN, Chaudhari GP, Udainiya S (2016) An assessment of ultra fine grained 316L stainless steel for implant applications. *J Acta biomaterialia* 30:408-419. doi:[10.1016/j.actbio.2015.10.043](https://doi.org/10.1016/j.actbio.2015.10.043)
41. Vafai K, Tien C (1981) Boundary and inertia effects on flow and heat transfer in porous media. *International Journal of Heat Mass Transfer* 24 (2):195-203. doi:[10.1016/0017-9310\(81\)90027-2](https://doi.org/10.1016/0017-9310(81)90027-2)
42. Vafai K *JJoFM* (1984) Convective flow and heat transfer in variable-porosity media. 147:233-259. doi:[10.1017/S002211208400207X](https://doi.org/10.1017/S002211208400207X)
43. Culbertson CT, Jacobson SC, Ramsey JM (2002) Diffusion coefficient measurements in microfluidic devices. *Talanta* 56 (2):365-373. doi:[10.1016/S0039-9140\(01\)00602-6](https://doi.org/10.1016/S0039-9140(01)00602-6)
44. Armour JC, Cannon JN (1968) Fluid flow through woven screens. *AIChE Journal* 14 (3):415-420. doi:[10.1002/aic.690140315](https://doi.org/10.1002/aic.690140315)
45. Kalyanasundaram S, Calhoun VD, Leong K (1997) A finite element model for predicting the distribution of drugs delivered intracranially to the brain. *Journal of Physiology-Regulatory, Integrative Comparative Physiology* 273 (5):R1810-R1821. doi:[10.1152/ajpregu.1997.273.5.R1810](https://doi.org/10.1152/ajpregu.1997.273.5.R1810)